arXiv:1603.01144v1 [astro-ph.EP] 3 Mar 2016

Ruling out the orbital decay of the WASP-43b exoplanet

Sergio Hoyer[1,2]
shoyer@iac.es

Enric Pallé [1,2]

Diana Dragomir [3]
and

Felipe Murgas [4,5]

Abstract

We present 15 new transit observations of the exoplanet WASP-43b in the i',g', and R filters with the 1.0-m telescopes of Las Cumbres Observatory Global Telescope (LCOGT) Network and the IAC80 telescope. We combine our 15 new light curves with 52 others from literature, to analyze homogeneously all the available transit light curves of this exoplanet. By extending the time span of the monitoring of the transits to more than 5 yr, and by analyzing the individual mid-times of 72 transits, we study the proposed shortening of the orbital period of WASP-43b. We estimate that the times of transit are well-matched by our updated ephemeris equation, using a constant orbital period. We estimate an orbital period change rate no larger than $\dot{P} = -0.02 \pm 6.6\ ms\ yr^{-1}$, which is fully consistent with a constant period. Based on the timing analysis, we discard stellar tidal dissipation factors $Q_* < 10^5$. In addition, with the modelling of the transits we update the system parameters: $a/Rs = 4.867(23)$, $i = 82.11(10)^\circ$ and $R_p/R_s = 0.15942(41)$, noticing a difference in the relative size of the planet between optical and NIR bands.

Subject headings: planetary systems – stars: individual (WASP43) — techniques: photometric – time - ephemeris

1. Introduction

Exoplanets with ultra short orbital periods ($\lesssim$ 1 d) are rare. Of the current $\sim$ 2000 confirmed exoplanets, 17 objects exhibit orbital periods of less than 1.3 days (based on the exoplanets.org public compilation: Han et al. 2014). The most extreme case of these objects is the Earth-size planet Kepler-178b, with an orbital period of only 8.5 h (Sanchis-Ojeda et al. 2013). Also, 8/17 of these planets have radii of $\leq$ 2 R_{Earth}, while the rest spans between 10 and 20 Earth radii with masses no larger than than 2 $M_{Jupiter}$, with the exception of WASP-18b which has an estimated mass of 10 $M_{Jupiter}$ (Hellier et al. 2009). One of these objects is WASP-43b (Hellier et al. 2011), a 0.93 $R_{Jupiter}$ size planet with a mass of 1.83 $M_{Jupiter}$, orbiting a K star in only 0.81 d (Gillon et al. 2012). Since its detection and con-

[1]Instituto de Astrofísica de Canarias, E-38205 La Laguna, Tenerife, Spain

[2]Universidad de La Laguna, Dpto. Astrofísica, E-38206 La Laguna, Tenerife, Spain

[3]The Department of Astronomy and Astrophysics, University of Chicago, 5640 S Ellis Ave, Chicago, IL 60637, USA

[4]Univer Grenoble Alpes, IPAG, F-38000 Grenoble, France

[5]CNRS, IPAG, F-38000 Grenoble, France

firmation by the Wide-Angle Search for Planets (WASP) group, this exoplanet has been studied intensively. For example, Gillon et al. (2012) reported an extended follow-up which included the observations of 20 transits with the 0.6 m TRAnsiting Planets and PlanetesImals Small Telescope (TRAPPIST) in a $I+z$ filter, 3 transits with the Euler telescope ($Gunn-r'$ band) and 7 secondary transits in the NIR (5 in the $Sloan-z'$ filter with TRAPPIST and 2 in narrow-band filters at the ESO Very Large Telescope). This work presented an estimation of the planet temperature, $T_{eq} = 1440\ K$, and a re-estimation the planet mass, 2 $M_{Jupiter}$. Shortly after, Wang et al. (2013) reported two secondary transit observations, deriving a $T_{planet} \sim 1850\ K$. Later, Blecic et al. (2014) also observed secondary transits with the Spitzer space telescope. Based on the central times of Gillon et al. (2012) transits and amateur data from the *Exoplanet Transit Database* (Poddaný et al. 2010), Blecic et al. (2014) reported for the first time a hint of change in the orbital period of $\dot{P} = -0.095 \pm 0.036\ s\ yr^{-1}$. Due to the closeness to its host star and the relative high stellar brightness ($V = 12.4\ mag$), WASP-43b is a very suitable target for atmospheric studies. One example of these studies is the transmission spectrum observations obtained with OSIRIS instrument at the 10.4-m Gran Telescopio Canarias (GTC) presented by Murgas et al. (2014). In addition to the tentative detection of NaI in the atmosphere of WASP-43b, Murgas et al. (2014) re-estimated the shortening of the orbital period to $\dot{P} = -0.15 \pm 0.06\ s\ yr^{-1}$ by including 5 new epochs in the analysis. Chen et al. (2014) presented 7 broad-band simultaneous observations (from g' to K filter) of a primary and a secondary transit using GROND instrument at the 2.2m MPG/ESO Telescope, reporting a possible difference between the transit depths of the optical and NIR light curves. Furthermore, using a re-analysis of Gillon et al. (2012) and amateur data, Chen et al. (2014) also calculated a non-negligible $\dot{P} = -0.09 \pm 0.04\ s\ yr^{-1}$. Recently, 6 transits and 5 eclipses observations with WFC3 instrument on board of the Hubble Space Telescope (HST) were presented to constrain the water abundance in the WASP-43b atmosphere (Kreidberg et al. 2014). These data were revisited by Stevenson et al. (2014) and Kataria et al. (2015) to map the thermal structure of the planet along the full orbital phase and to fit a circulation model of the planet, respectively. Along with these studies on the exoplanet atmosphere, Stevenson et al. (2014) reported high precision mid-times for each transit. Additional transits were also reported by Maciejewski et al. (2013), 1 epoch in R and 1 without filter, and Ricci et al. (2015), 7 observations of 6 different epochs in the R, V and i' filters, giving a a new value of $\dot{P} = -0.03 \pm 0.03\ s\ yr^{-1}$. During the writing of this work, 9 new transits observations of WASP-43b were reported by Jiang et al. (2015). Combining their data to the literature transits, they found that the amplitude of orbital decay is consistent with previous works, $\dot{P} = -0.029 \pm 0.008\ s\ yr^{-1}$ and therefore, a slow decreasing rate of the period was not discarded.

Here, we present a total of 15 new transit observations on 9 different epochs. Of these, 14 transits were obtained with Las Cumbres Observatory Global Telescope (LCOGT) Network while one transit was observed with the 0.8m IAC80 Telescope. Combining these new data and all the literature transits available for WASP-43b, we perform an homogeneous analysis of the light curves, with special focus in the transit times, to probe the proposed orbital decay. Along with the timing studies, we also revisited the system and transit parameters of WASP-43b. In Section 2 we present our observations, in Section 3 we describe the modelling of the transits, in Section 4 we present the timing analysis of the transits divided in two parts: in Section 4.1 we present the time analysis of the 58 transits analyzed in this work while in Section 4.2 we include into the analysis additional timing information available for this planet. In Section 5 we use our timing results to constrain the tidal dissipation efficiency of WASP-43. Finally in Section 6 we present our conclusions.

2. Observations

We present 15 new observations, obtained in 9 different transit epochs, of the exoplanet WASP-43b. Of these, 6 events were observed simultaneously in the i' and g' filters with the 1.0-m LCOGT Network, other two transits were observed only with the g' or the i' filter also at the 1.0-m LCOGT, and one additional epoch was observed in the R band with the 0.8-m IAC80 tele-

scope at Teide Observatory, Spain. The node of the LCOGT Network located at Cerro Tololo Interamerican Observatory (CTIO) in Chile was used to observed 6 of the epochs. The 1.0-m telescopes at the CTIO site are equipped with Sinistro cameras, with a Field-of-View (FoV) of 27×27 $arcmin^2$, a pixel size of 0.389 $arcsec$, and a readout time of 51 s without binning. Other two epochs were observed using the telescopes of the node at the South African Astronomical Observatory (SAAO). This node was equipped with a Sbig camera with a FoV of 16×16 $arcmin^2$, a pixel scale of 0.232 $arcsec$, and a readout time of 15.5 s when using the 2×2 binning mode. Some of the observations were taken with the telescopes defocused in order to increase the number of counts per object without reaching the non-linearity regime of the detectors. The egress of the transit in 2014-May-26 was lost due to bad weather conditions at CTIO.

The transit at IAC80 telescope was observed using the CAMELOT instrument. CAMELOT has a collector area of 2048x2048 $pixels^2$ with two readout amplifier channels, a FoV of 10.4x10.4 $arcmin^2$ and a pixel scale of 0.304 $arcsec$. The observation was performed using the 500 KHz readout speed in both channels without binning, having thus a readout time of 4.4 s. Our last observation was executed in 2016-Feb-04 and corresponds to the transit epoch 2329 (using as E=0 the reference epoch from Hellier et al. (2011)). With this observation we extend the monitoring of the WASP-43b transits to 5.2 yr. The observing log of each observation is shown in Table 1.

2.1. Reduction and Photometry

All images were processed using the pipeline described in Brown et al. (2013). Briefly, the entirely automated procedure includes bad-pixel masking, bias subtraction, dark subtraction, flat field correction and astrometric solution. We used custom made Python pipelines to perform differential aperture photometry on the target and several stars in the FoV are used as reference. We choose the best reference stars by identifying the objects which produce the lowest RMS in the out-of-transit (oot) data. The size of the aperture and the ring used to measure the sky background were also chosen with the same RMS criteria. The final aperture radii were on the range of the 13-20 pixels, and the radii and widths of the sky rings were between 18-25 and 10-20 pixels, respectively.

2.2. Literature transits

We have included in our homogeneous analysis all the light curves available in the literature. We used 23 transits from Gillon et al. (2012), 2 transits from Maciejewski et al. (2013), the 7 light curves from Chen et al. (2014) of the epoch=499 transit, the 5 transits from Murgas et al. (2014) and the 7 light curves from Ricci et al. (2015) (obtained in 6 different epochs). The epoch and filter of each transit is shown in Table 2. We also fit the 8 transits recently reported Jiang et al. (2015) in order to include their epochs in our timing analysis although we did not use it in Section 3 to derive the final system parameters.

[ht]

3. Modelling

We used the *TAP* package (Gazak et al. 2012) for the simultaneous modelling of all the light curves. This package allows to fit for orbital and transit parameters using the analytic function of Mandel & Agol (2002) to describe the exoplanetary transits. TAP also incorporates the wavelet method of Carter & Winn (2009) to estimate the correlated noise in the light curves and the Markov Chain Monte Carlo (MCMC) approach to calculate the uncertainties of the fitted parameters. In particular the parameters subject to be fitted are: orbital period (P), inclination (i), eccentrycity (e), longitude of the periastron (w), relative distance to the host star (a/R_s), planet-to-star radii ratio (R_p/R_s), transit mid-time (T_c) and the coefficients of a limb-darkening quadratic law (u_1 and u_2). Furthermore, this version also allows to fit for a time dependent linear function (i.e. F_{slope} and F_{shift}) in addition to the noise parameters (σ_{red} and σ_{white}) from the wavelet method, assuming that the correlated noise can be described by a $1/f^{\gamma}$ function, where f is the frequency and γ is assumed to be equal to 1 (see Carter & Winn (2009) for details). Two different methodologies were employed.

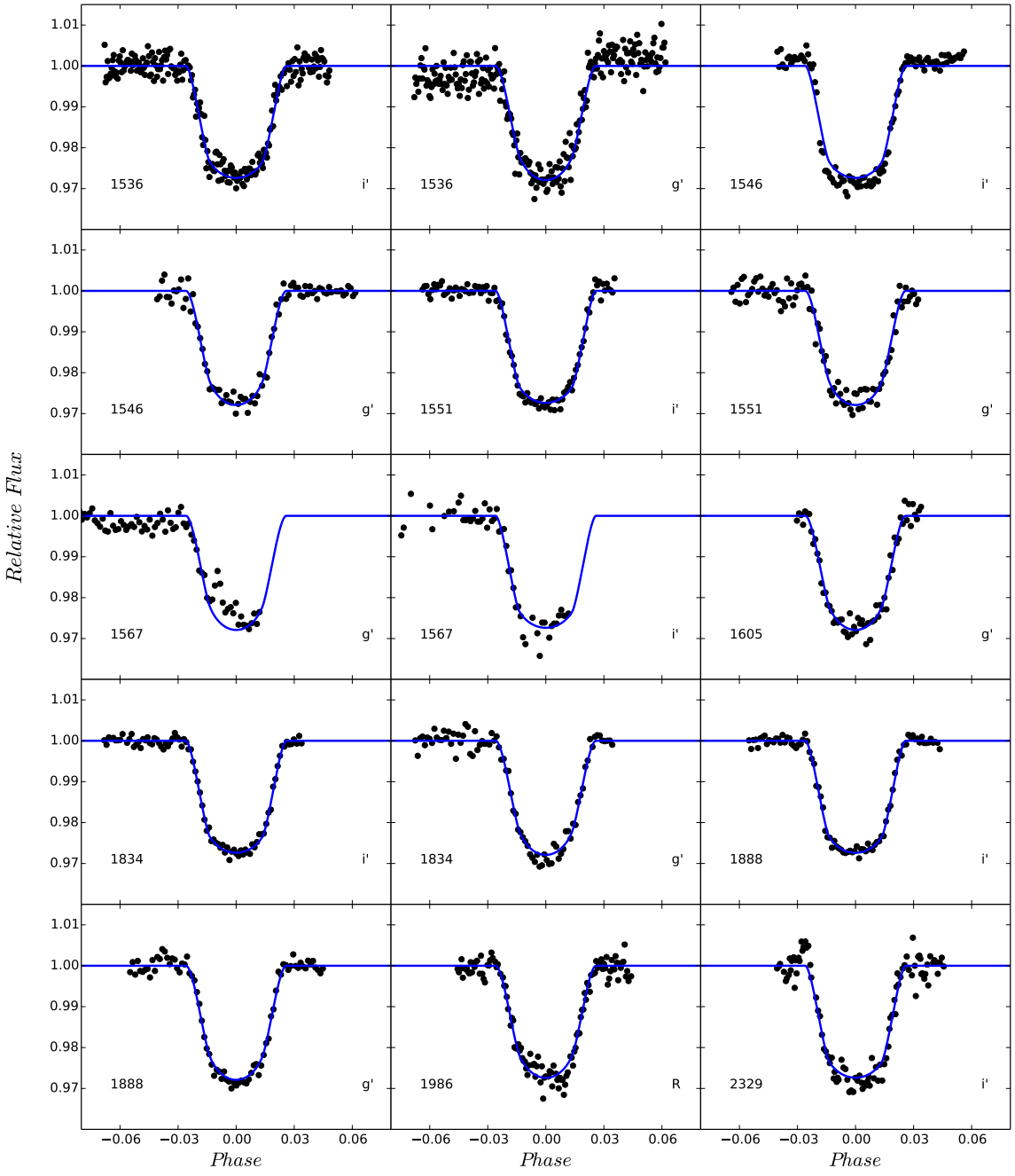

Fig. 1.— The 15 new light curves presented in this work (black points) and the best-fitting model obtained in Section 3.1 (blue solid line). The epoch and the filter of the transit observation is shown on the left and right bottom corner of each panel, respectively. All the light curves were obtained with LCOGT Network except for the transit E=1986 which was observed with the IAC80 Telescope.

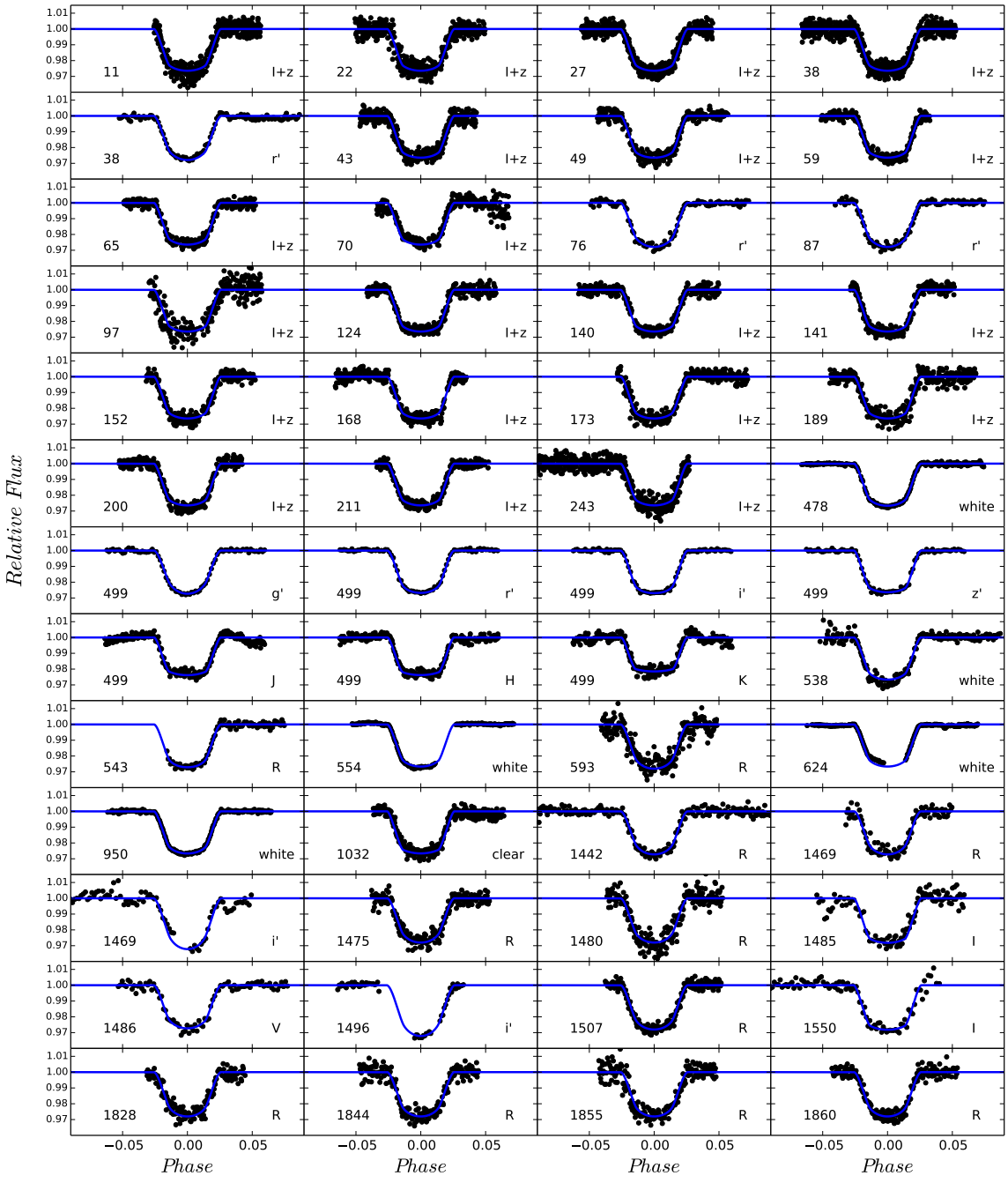

Fig. 2.— We show all the literature transit light curves analyzed in this work and the best model we obtained in Section 3.1. The epoch and filter of the transit observation is shown on the left and right bottom corner of each panel, respectively.

Table 1
Log of the observations.

Date [a] (yyyymmdd)	Epoch [b]	Site	Camera / Intrum. ID	Filter	Exposure (s)	Binning (pix × pix)	Airmass
20140501	1536	SAAO	Sbig / kb75	g'	30	2x2	1.1-1.82
		SAAO	Sbig / kb70	i'	30	2x2	1.1-1.64
20140509	1546	CTIO	Sinistro / fl04	g	60	1x1	1.1-1.06-1.14
		CTIO	Sinistro / fl03	i'	30	1x1	”
20140513	1551	CTIO	Sinistro / fl03	g	45	1x1	1.07-1.37
		CTIO	Sinistro / fl02	i'	40	1x1	”
20140526	1567	CTIO	Sinistro / fl04	i'	60	1x1	1.09-1.61
		CTIO	Sinistro / fl03	g'	70	1x1	”
20140626	1605	CTIO	Sinistro / fl04	g'	45	1x1	1.28-1.89
20141229	1834	CTIO	Sinistro / fl04	g'	60	1x1	1.67-1.10
		CTIO	Sinistro / fl03	i'	55	1x1	”
20150211	1888	CTIO	Sinistro / fl04	g'	65	1x1	1.24-1.06
		CTIO	Sinistro / fl03	i'	55	1x1	”
20150502	1986	Teide	CAMELOT	R	50	1x1	1.27-1.99
20160204	2329	SAAO	Sbig / kb76	i'	30	2x2	1.29-1.08

[a]corresponds to the date stamp in the header of the first frame of the run.

[b]transit epoch of the observation, here E=0 corresponds to the epoch reported by Hellier et al. (2011)

3.1. Method 1: Joint modelling with free R_p/R_s

In order to explore any variation as a function of wavelength, in a first step we grouped the transits according to the filter and telescope and fit for R_p/R_s and (u_1,u_2) on each set of light curves. We modelled i and a/R_s simultaneously in all the transits, fixing P to 0.81347385 d from Murgas et al. (2014), and $e = w = 0$. The midtime of each transit (T_c) and the rest of the parameters were left free to vary individually on each transit. We used 10 MCMC chains of 10^5 links each. The resulting parameters were obtained from the median of the posterior distributions and its respective uncertainties from the 16 and 84 percentile levels. In Fig. 1 and 2, we show each transit light curve and its final model for the LCOGT and literature transits, respectively, and in Table 2 we show the parameters obtained using *TAP*. In Figure 3 we show the values of R_p/R_s for each group of light curves, which present a very good agreement for the optical filters. Only the two transits in I and i' of Ricci et al. (2015) deviate from the rest of the optical band transits, probably due to the low quality of these light curves. We also notice that the NIR transits depths (J-,H- and K- bands) also deviate significantly from the optical values. Chen et al. (2014) reported a similar deviation in the z'-,H- and K- bands, but their differences were not statistically significant. A multi-epoch study in NIR bands would be needed to confirm this finding.

3.2. Method 2: Joint modelling with common R_p/R_s

To take advantage of the large amount of data we have, we use all the light curves in the modelling to refine the final planet parameters. We repeated the method described in Section 3.1 but this time fitting R_p/R_s simultaneously for all the optical and the NIR transits from Chen et al. (2014). Here we remove some transits from the joint modelling since we have identified in the previous step that its respective R_p/R_s values deviates considerably from the rest of the transits. In particular, we removed from the simultaneous modelling of R_p/R_s the i' and I transits from Ricci et al. (2015), and the E=538, 554 and 624 transits from Murgas et al. (2014) whose transit depths were strongly affected by bad weather and/or technical issues during observation. We have not included in this step the data from Jiang et al. (2015) since these transits were only available at a final stage of this work. As in method 1, the u_1 and u_2

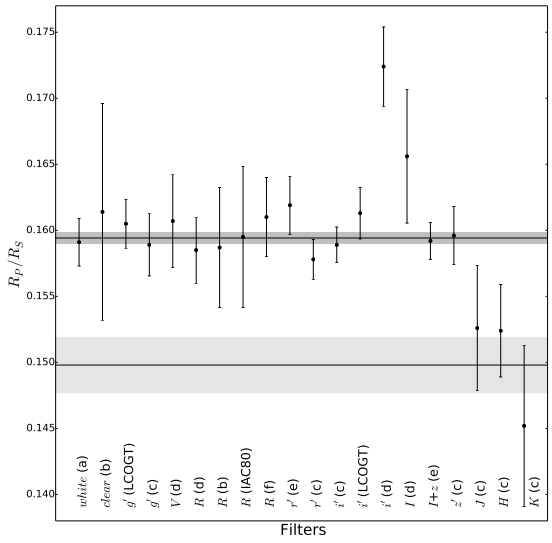

Fig. 3.— Here we show the values of R_p/R_s obtained for each set of light curves modelled independently. We label each *set* using the filter and author as follow: (a) Murgas et al. (2014), (b) Maciejewski et al. (2013), (c) Chen et al. (2014), (d) Ricci et al. (2015), (e) Gillon et al. (2012), (f) Jiang et al. (2015) and (LCOGT) and (IAC80) are from this work. The top black solid line and the grey region correspond to the resulting value, and its errors, of the joint modelling of all the light curves (Section 3.2). We unlinked from the joint modelling the i' and I from (d), which deviate noticeably from the rest of the sets (see text for details). The lower flat line shows the result from the joint modelling of the NIR transits: J, H and K from (c).

coefficients are fitted by groups.

By doing this we obtained $Rp/Rs = 0.15942 \pm 0.00041$ and $R_p/R_s = 0.1498 \pm 0.0021$ for the optical and NIR bands, respectively. Additionally, we obtained $i = 82.11 \pm 0.10$, and $a/R_s = 4.867^{+0.023}_{-0.025}$ from all the light curves. As expected, the values of a/R_s and i do not differ from those obtained before, but the *optical* R_p/R_s is one order of magnitude more precise by using the joint modelling. Regarding the mid-times of each transit we obtained values fully consistent between the two methods. Our derived R_p/R_s is also consistent with the values reported by Murgas et al. (2014), Stevenson et al. (2014) and Jiang et al. (2015): $0.15988^{+0.00133}_{-0.00145}$, 0.15948 ± 0.00004, and 0.15929 ± 0.00045, respectively. On the other hand, the R_p/R_s derived from NIR transits deviates significatively from these measurements (see Figure 3), even though Stevenson et al. (2014) value is based on data which cover the J- and H-filters.

4. Timing Analysis

For the modelling of our light curves we use the mid-exposure time of each frame recorded in Julian Days (UTC). Later on, we transform the resulting T_c for each transit to Barycentric Julian Days (BJD) in the Barycentric Dynamical Time (TDB) standard as suggested by Eastman et al. (2010). For the literature values we also performed the necessary transformation of the central times of their original time standard to BJD_{TDB}. As mentioned before, we have obtained simultaneous observations of 6 transits epochs with two 1-m LCOGT telescopes (3 additional transits were not observed simultaneously). The mid-times we obtained for each of the simultaneous observations are consistent within the errors, with the exception of the transits of epoch 1834, which deviates by 1.5σ (very likely due to an underestimated error and/or unaccounted systematics in the g' transit). Furthermore, our retrieved mid-times for the literature data are also consistent with the original reported values. The average difference between those mid-times is only $\sim 0.35\sigma$.

4.1. Timing results from the mid-times of our homogeneous analysis

To adjust the mid-times of the 67 transits obtained in Section 3, we used a linear ephemeris equation of the form:

$$T(E) = T_0 + E \times P, \quad (1)$$

where the central time of the transit T_c at epoch E, is calculated with respect to the reference time T_0 using the orbital period P. To update the linear ephemeris we used the `scipy.optimize` module of Python and the `emcee` MCMC sampler implementation (Foreman-Mackey et al. 2013). We fit for P and T_0, and estimate its uncertainties using 1000 walkers with 5000 links each. In a first step, we identified that the two transits of epoch 1469 deviate by more than 147 s. As these transits were

not included in the analysis on the original publication (private communication with the author) we also decided to remove them from the timing analysis. After repeating the MCMC analysis for the rest of the 65 transits, we obtained the following ephemeris equation:

$$T(E) = 2455528.868602(47) + E \times 0.813474077(54), \quad (2)$$

where the quoted values and their uncertainties (in parenthesis) were adopted from the 50%, 16% and 84% percentiles of the drawn posterior distributions, respectively. The RMS of the timing residuals is 37 s. The χ^2 of this fit is 121, the reduced-χ^2 is 1.93 and the Bayesian Information Criterion ($BIC = 2log(\nu) + \chi^2$, where ν is the number of degrees of freedom) is 130.

To probe for orbital decay, i.e. a shortening of the orbital period with time, we also explore the possibility that the transit times can be adjusted by including a quadratic additional term. Therefore we fit the transit times using, as in Adams et al. (2010), the following ephemeris equation:

$$T_c(E) = T_0 + E \times P + \frac{1}{2}\delta P \times E(E-1), \quad (3)$$

where the new term δP corresponds to the change rate of the orbital period per $epoch^{-2}$ ($\delta P = \dot{P} \times P$). Using the same procedure as in the linear case, the resulting values of this quadratic fit are: $\delta P = (0.38 \pm 1.90) \times 10^{-10}$ d $epoch^{-2}$, $P = 0.81347404(19)$ d and $T_0(BJD_{TDB}) = 2455528.868610(66)$. This new δP, which can be translated to $\dot{P} = 1.5 \pm 7.3$ ms yr^{-1}, is fully consistent with a constant orbital period.

This quadratic fit has a RMS of 37 s, a χ^2 of 121, a reduced-χ^2 of 1.96 and a $BIC_{quad} = 134$. These numbers suggest that the linear equation is the most likely function to describe the transits of WASP-43b.

4.2. Including additional transit mid-times

Although we could not include in our modelling the transit light curves presented in Hellier et al. (2011) and Stevenson et al. (2014), we check our results by using their published mid-times. Since we do not have any common transit as a comparison point we use their reported uncertainties without scaling them. Thus, we repeat the fitting process using a total of 72 transits, resulting in the most comprehensive study of the WASP-43b transits to date. We obtain in this case a $\dot{P} = -0.02 \pm 6.6$ ms yr^{-1}, consistent again with the constant orbital period case. Furthermore, in this case the BIC also favors the linear equation ($BIC_{lin} = 353$) over a non-constant period scenario ($BIC_{quad} = 358$). Therefore, this new value of $\dot{P}$ rules out definitively a rapid or slowly period decay of the WASP-43b exoplanet. Is worth mentioning that our monitoring includes a transit in the epoch=2329, which extends the monitoring 381 d beyond the last epoch reported by Jiang et al. (2015), totaling more than 5 years of follow-up. Long term monitoring is critical to probe small amplitude timing variations in the transits of exoplanets (e.g. see Fig.14 of Birkby et al. 2014; Hoyer et al. 2016).

Finally, using the 72 transits we calculate the updated linear ephemeris function:

$$T(E) = 2455528.868634(46) + E \times 0.813473978(35), \quad (4)$$

where the RMS of the timing residuals is 35 s, the reduced-$\chi^2 = 4.9$ and the $BIC = 353$.

The *Observed minus Calculated* diagram of the transit mid-times based on this linear fit is shown in Figure 4, where the open points represent the literature transits analyzed in Section 3, the gray points are from Hellier et al. (2011) and Stevenson et al. (2014), and the red points correspond to the new transits presented in this work. The red region corresponds to the 1σ uncertainties of the linear fit. In this Figure the fitted quadratic function based on the 72 transits and its 1σ errors are represented by the solid black line and the blue light region, respectively. For comparison we plot with the dashed line the decay function obtained by Jiang et al. (2015). It is clear that despite the errors in the mid-times and the dispersion of the residuals, the most recent epochs do not follow the proposed $\dot{P} = -28$ ms yr^{-1}.

5. Constraints on Q*

Stellar tidal dissipation, usually characterized through the quality or efficiency factor, Q_*, can drives the planet orbital motion and determine, for example, the life time before it collides with its host star (Levrard et al. 2009; Penev et al. 2012). Therefore, empirical constraints of Q_* are relevant for models of formation and evolution of close-in

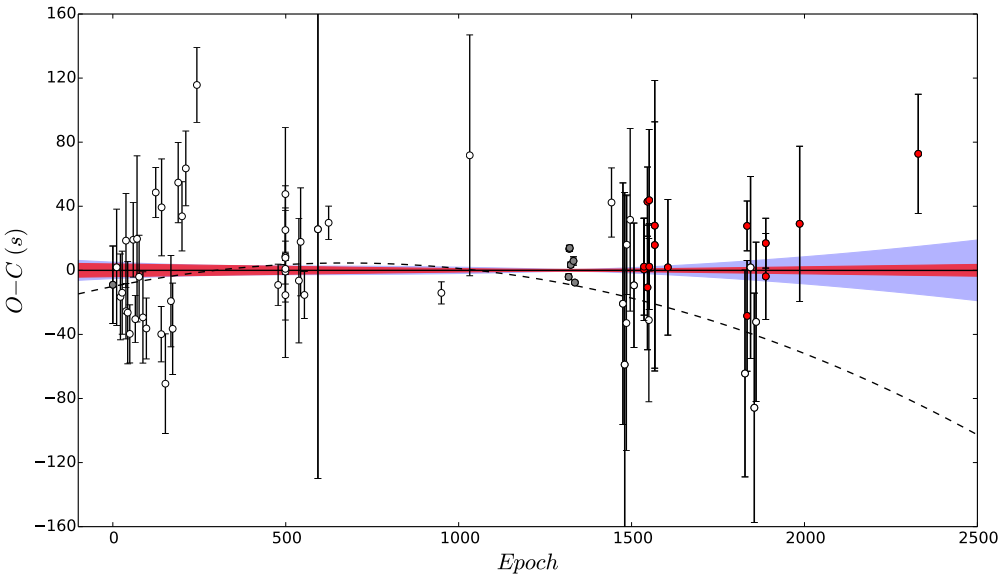

Fig. 4.— *Observed minus Calculated* diagram of 72 transit mid-times of WASP-43b. The timing residuals obtained from the 65 light curves analyzed in this work are shown. The white and red points correspond to the literature and the new transits presented in this work, respectively, while the gray points represent the mid-times reported by Hellier et al. (2011) and Stevenson et al. (2014). The timing residuals are based on our updated linear ephemeris equation (Eq. 4), and the red region represents its $\pm 1\sigma$ errors. The solid black line and the light blue region represent the fitted quadratic function and its uncertainties, respectively. The dashed line corresponds to the changing period function reported by Jiang et al. (2015).

exoplanets. Measuring the shortening of orbital periods of transiting exoplanets is a direct way to estimate Q_* (e.g. Matsumura et al. 2010; Penev et al. 2012; Birkby et al. 2014; Hoyer et al. 2016). For WASP-43, previous studies pointed to Q_* between $10^4 - 10^{10}$ (Hellier et al. 2009; Blecic et al. 2014; Jiang et al. 2015). In particular, using the equations in Birkby et al. (2014), we calculate that the previous reported $\dot{P} = -30\ ms\ yr^{-1}$ implies a $Q_* \approx 4 \times 10^4$ and therefore a $T_{shift} \approx 170\ s$ in the time arrival of the transits after 5 years. Such large time deviation is not detected in our $O-C$ diagram (Figure 4). Now, based on the uncertainties of our estimation of $\dot{P}$ ($\pm 6.6\ ms\ yr^{-1}$), we derive a $Q_* \approx 2 \times 10^5$ and a $T_{shift} \approx 39\ s$ after 5 yr which is is consistent with our transit timing, considering the $RMS = 35\ s$ of the time residuals we obtained. Larger values of Q_* result, after 5 yr, in time deviations of smaller amplitude than the dispersion of the $O-C$. Thus, for WASP-43 we can discard Q_* values smaller than 10^5. With this precision in $\dot{P}$, and if the dispersion of residuals of the transit times continues in the 30 s level after 5 additional years (i.e. around the epoch 4500), it would be possible to probe the $Q_* < 10^6$ limit.

6. Conclusions

With the timing analysis of 72 transit of WASP-43b, we have estimated that the change rate of the orbital period is consistent with zero. By extending the time span of the monitoring to more than 5 yr, i.e. to 2329 orbits, we have constrained the orbital decay to $\dot{P} = -0.02 \pm 6.6\ ms\ yr^{-1}$, which is 3 order smaller than values previously reported. Based on our estimation of $\dot{P}$, we can discard $Q_* < 10^5$ for WASP-43. Finally, by fitting together the optical transit light curves we have a re-estimation of the relative size of the planet, $R_p/R_s = 0.15942 \pm 0.00041$, a value also consistent with previous studies. We also found a difference between the R_p/R_s derived from optical and NIR filters. We note that the HST data of Stevenson et al. (2014) cover the $1.1 - 1.7 \mu m$ wavelength

range, i.e, it includes part of the J and H bands, and their reported R_p/R_s is fully consistent with our *optical* results. Thus, additional NIR observations are needed to state definitively this discrepancy.

This work makes use of observations made in LCOGT network and the IAC80 telescope operated on the island of Tenerife by the IAC in the Spanish Observatorio del Teide. SH acknowledges financial support from the Spanish Ministry of Economy and Competitiveness (MINECO) under the 2011 Severo Ochoa Program MINECO SEV-2011-0187. This work is partly financed by the Spanish Ministry of Economics and Competitiveness through projects ESP2013-48391-C4-2-R and ESP2014-57495-C2-1-R. FM acknowledges the support of the French Agence Nationale de la Recherche (ANR), under the program ANR-12-BS05-0012 Exo-atmos.

REFERENCES

Adams, E. R., López-Morales, M., Elliot, J. L., Seager, S., & Osip, D. J. 2010, ApJ, 721, 1829

Birkby, J. L., Cappetta, M., Cruz, P., et al. 2014, Monthly Notices of the Royal Astronomical Society, 440, 1470

Blecic, J., Harrington, J., Madhusudhan, N., et al. 2014, ApJ, 781, 116

Brown, T. M., Baliber, N., Bianco, F. B., et al. 2013, PASP, 125, 1031

Carter, J. A., & Winn, J. N. 2009, ApJ, 704, 51

Chen, G., van Boekel, R., Wang, H., et al. 2014, Astronomy & Astrophysics, 563, A40

Eastman, J., Siverd, R., & Gaudi, B. S. 2010, PUBL ASTRON SOC PAC, 122, 935

Foreman-Mackey, D., Hogg, D. W., Lang, D., & Goodman, J. 2013, Publications of the Astronomical Society of the Pacific, 125, 306

Gazak, J. Z., Johnson, J. A., Tonry, J., et al. 2012, Advances in Astronomy, 2012, 1

Gillon, M., Triaud, A. H. M. J., Fortney, J. J., et al. 2012, Astronomy & Astrophysics, 542, A4

Han, E., Wang, S. X., Wright, J. T., et al. 2014, Publications of the Astronomical Society of the Pacific, 126, 827

Hellier, C., Anderson, D. R., Cameron, A. C., et al. 2009, Nature, 460, 1098

—. 2011, Astronomy & Astrophysics, 535, L7

Hoyer, S., López-Morales, M., Rojo, P., Minniti, D., & Adams, E. R. 2016, MNRAS, 455, 1334

Jiang, I.-G., Lai, C.-Y., Savushkin, A., et al. 2015, ArXiv e-prints, arXiv:1511.00768

Kataria, T., Showman, A. P., Fortney, J. J., et al. 2015, ApJ, 801, 86

Kreidberg, L., Bean, J. L., Désert, J.-M., et al. 2014, ApJ, 793, L27

Levrard, B., Winisdoerffer, C., & Chabrier, G. 2009, APJL, 692, L9

Maciejewski, G., Puchalski, D., Saral, G., et al. 2013, Information Bulletin on Variable Stars, 6082, 1

Mandel, K., & Agol, E. 2002, The Astrophysical Journal, 580, L171

Matsumura, S., Peale, S. J., & Rasio, F. A. 2010, ApJ, 725, 1995

Murgas, F., Pallé, E., Osorio, M. R. Z., et al. 2014, Astronomy & Astrophysics, 563, A41

Penev, K., Jackson, B., Spada, F., & Thom, N. 2012, ApJ, 751, 96

Poddaný, S., Brát, L., & Pejcha, O. 2010, New Astronomy, 15, 297

Ricci, D., Ramón-Fox, F. G., Ayala-Loera, C., et al. 2015, Publications of the Astronomical Society of the Pacific, 127, 143

Sanchis-Ojeda, R., Rappaport, S., Winn, J. N., et al. 2013, ApJ, 774, 54

Stevenson, K. B., Desert, J.-M., Line, M. R., et al. 2014, Science, 346, 838

Wang, W., van Boekel, R., Madhusudhan, N., et al. 2013, ApJ, 770, 70

This 2-column preprint was prepared with the AAS LaTeX macros v5.2.

TABLE 2

FITTED CENTRAL TIME AND PLANET-TO-STAR RADIUS RATIO OF THE 67 TRANSITS.

Epoch	Filter	T_C $(BJD_{TDB} - 2450000)$	R_p/R_s	Reference
11	I+z	5537.81687 ± 0.00042	0.1592 ± 0.0014	(a)
22	I+z	5546.76487 ± 0.00031	"	"
27	I+z	5550.83227 ± 0.00030	"	"
38	I+z	5559.78035 ± 0.00020	"	"
43	I+z	5563.84771 ± 0.00037	"	"
49	I+z	5568.72840 ± 0.00021	"	"
59	I+z	5576.86382 ± 0.00027	"	"
65	I+z	5581.74409 ± 0.00017	"	"
70	I+z	5585.81204 ± 0.00060	"	"
97	i+z	5607.77519 ± 0.00022	"	"
124	I+z	5629.73997 ± 0.00018	"	"
140	I+z	5642.75453 ± 0.00020	"	"
141	I+z	5643.56892 ± 0.00035	"	"
152	I+z	5652.51586 ± 0.00036	"	"
168	I+z	5665.53204 ± 0.00033	"	"
173	I+z	5669.59921 ± 0.00033	"	"
189	I+z	5682.61585 ± 0.00029	"	"
200	I+z	5691.56382 ± 0.00025	"	"
211	I+z	5700.51238 ± 0.00027	"	"
243	I+z	5726.54415 ± 0.00027	"	"
38	r'	5559.78086 ± 0.00034	$0.1619^{+0.0021}_{-0.0023}$	"
76	r'	5590.69261 ± 0.00030	"	"
87	r'	5599.64053 ± 0.00033	"	"
543	R	5970.58521 ± 0.00039	$0.1587^{+0.0049}_{-0.0042}$	(b)
593	R	6011.2590 ± 0.0010	$0.1610^{+0.0030}_{-0.0030}$	(f)
1032	clear	6368.37461 ± 0.00087	0.1614 ± 0.0082	"
499	g'	5934.79197 ± 0.00018	0.1589 ± 0.0024	(c)
499	r	5934.79216 ± 0.00011	$0.1578^{+0.0014}_{-0.0016}$	"
499	i'	5934.79224 ± 0.00012	$0.1589^{+0.0015}_{-0.0012}$	"
499	z'	5934.79244 ± 0.00016	$0.1596^{+0.0024}_{-0.0020}$	"
499	J	5934.79270 ± 0.00048	0.1526 ± 0.0048	"
499	H	5934.79225 ± 0.00033	$0.1524^{+0.0036}_{-0.0034}$	"
499	K	5934.79214 ± 0.00062	$0.1452^{+0.0060}_{-0.0062}$	"
478	white	5917.70909 ± 0.00015	0.1591 ± 0.0018	(d)
538	white	5966.51756 ± 0.00045	"	"
554	white	5979.53304 ± 0.00017	"	"
624	white	6036.47674 ± 0.00012	"	"
950	white	6301.66875 ± 0.00008	"	"
1442	R	6701.89860 ± 0.00025	0.1585 ± 0.0025	(e)
1469	R	6723.86516 ± 0.00060	"	"
1469	i'	6723.86378 ± 0.00080	0.1724 ± 0.0030	"
1485	I	6736.87711 ± 0.00092	0.1656 ± 0.0051	"
1486	V	6737.69115 ± 0.00036	$0.1607^{+0.0033}_{-0.0037}$	"
1496	i'	6745.82607 ± 0.00066	0.1724 ± 0.003	"
1550	I	6789.75294 ± 0.00059	0.1656 ± 0.0051	"
1475	R	6728.74251 ± 0.00049	$0.1610^{+0.0030}_{-0.0030}$	(f)
1480	R	6732.80944 ± 0.00069	"	"
1507	R	6754.77381 ± 0.00025	"	"
1828	R	7015.89832 ± 0.00042	"	"
1844	R	7028.91467 ± 0.00037	"	"

TABLE 2—*Continued*

Epoch	Filter	T_C $(BJD_{TDB} - 2450000)$	R_p/R_s	Reference
1855	R	7037.86187 ± 0.00046	”	”
1860	R	7041.92986 ± 0.00032	”	”
1536	i'	6778.36469 ± 0.00035	$0.1613^{+0.0021}_{-0.0018}$	(g)
1546	i'	6786.49928 ± 0.00045	”	”
1551	i'	6790.56680 ± 0.00031	”	”
1567	i'	6803.58254 ± 0.00089	”	”
1834	i'	7020.78023 ± 0.00018	”	”
1888	i'	7064.70770 ± 0.00018	”	”
2329	i'	7423.45037 ± 0.00043	”	”
1536	g'	6778.36467 ± 0.00037	$0.1605^{+0.0020}_{-0.0017}$	(g)
1546	g'	6786.49990 ± 0.00025	”	”
1551	g'	6790.56728 ± 0.00051	”	”
1567	g'	6803.58268 ± 0.00105	”	”
1605	g'	6834.49439 ± 0.00049	”	”
1834	g'	7020.77958 ± 0.00040	”	”
1888	g'	7064.70746 ± 0.00031	”	”
1986	R	7144.42829 ± 0.00056	$0.1595^{+0.0052}_{-0.0055}$	”

NOTE.—Results of the modelling of 67 transit light curves of WASP-43b (see Section 3.1). The reference of each transit corresponds to: (a) Gillon et al. (2012), (b) Maciejewski et al. (2013), (c) Chen et al. (2014), (d) Murgas et al. (2014), (e) Ricci et al. (2015), (f) Jiang et al. (2015) and (g) this work.

TABLE 3
FINAL RESULTS.

Parameter	value	$\pm 1\sigma$
R_p/R_s	0.15942	0.00041
i (degrees)	82.11	0.10
a/R_s	4.867	0.023
P (d)	0.813473978	0.000000035
T_0 (BJD_{TDB})	2455528.868634	0.000046

NOTE.—Final results of the joint modelling of the light curves (Section 3.2) and the timing analysis of the transits (Section 4.1).